Probing dynamics of a two-dimensional dipolar spin ensemble using single qubit sensor

Kristine Rezai[1,3], Soonwon Choi[2], Mikhail D. Lukin[1], Alexander O. Sushkov[3,4,5]

[1]Department of Physics, Harvard University, Cambridge, MA 02138, USA

[2]Department of Physics, Massachusetts Institute of Technology, Cambridge, MA 02142, USA

[3]Department of Physics, Boston University, Boston, MA 02215, USA

[4]Department of Electrical and Computer Engineering, Boston University, Boston, MA 02215, USA

[5]Photonics Center, Boston University, Boston, MA 02215, USA

*To whom correspondence should be addressed; e-mail: asu@bu.edu

Abstract

Understanding the thermalization dynamics of quantum many-body systems at the microscopic level is among the central challenges of modern statistical physics. Here we experimentally investigate individual spin dynamics in a two-dimensional ensemble of electron spins on the surface of a diamond crystal. We use a near-surface NV center as a nanoscale magnetic sensor to probe correlation dynamics of individual spins in a dipolar interacting surface spin ensemble. We observe that the relaxation rate for each spin is significantly slower than the naïve expectation based on independently estimated dipolar interaction strengths with nearest neighbors and is strongly correlated with the timescale of the local magnetic field fluctuation. We show that this anomalously slow relaxation rate is due to the presence of strong dynamical disorder and present a quantitative explanation based on dynamic resonance counting. Finally, we use resonant spin-lock driving to control the effective strength of the local magnetic fields and reveal the role of the dynamical disorder in different regimes. Our work paves the way towards microscopic study and control of quantum thermalization in strongly interacting disordered spin ensembles.

Quantum thermalization connects statistical physics with unitary quantum mechanics. Recent technological developments in quantum information science have enabled detailed studies of isolated quantum systems, revealing a variety of novel phenomena such as the role of entanglement in thermalization [1, 2, 3], the localization in the absence of strong disorder [4], non-equilibrium phases [5, 6, 7, 3, 8, 9], and quantum many-body scarring [10, 11, 12]. Despite this progress, one of the key open questions in this

field is the nature of microscopic relaxation dynamics in presence of dynamical disorder and long-range interactions [13]. The majority of existing studies focus on ensemble measurements in systems dominated by static disorder [14, 15, 16, 17, 18, 19]. However ensemble averaging can conceal important features of microscopic dynamical evolution [20, 21], and in many noisy real-world quantum systems disorder is dynamic, exhibiting non-trivial time-dependence. Another important factor is system dimensionality and its interplay with the distance scaling of interactions. The long-range $1/r^3$ dipolar spin interaction implies that a two-dimensional system should be localized according to the single-particle Anderson model [22], but delocalized according to the many-body interacting treatment [23, 24, 25, 26, 27]. In addition to fundamental interest, understanding the dynamics of two-dimensional systems is important for quantum sensing applications, since such systems can be positioned in close proximity to a sensing target [28, 29].

We experimentally investigate spin transport dynamics of a two-dimensional ensemble of randomly-positioned spin-1/2 qubits with long-range magnetic dipolar interactions [29]. Naïvely, one could expect that the spin exchange (flip-flop) component of dipolar interactions limits the lifetime of local polarization of spins. Our observation, however, reveals a surprising finding that the spin lifetime is, in fact, significantly longer than independently-estimated interaction strengths. We attribute this anomalously-slow spin relaxation dynamics to the interplay between interactions and strong time-dependent local disorder, created by hyperfine fields of proximal nuclear spins. We control the effective strength of this disorder and observe the corresponding scaling of the relaxation rate. We present a theoretical model, based on dynamic resonance-counting arguments, which is in quantitative agreement with our experimental observations and reveals a universal scaling collapse of our data for different values of disorder strengths and correlation times.

Our experimental platform is the ensemble of paramagnetic two-level systems on the surface of a diamond crystal, fig. 1 (a) [30, 31, 32]. These surface spins are associated with electron spin $S = 1/2$ impurities that are not optically active. Their exact nature is subject to ongoing investigation, but they are likely localized defect surface states [33, 34]. Due to faster decoherence of shallow NV centers [35, 36, 37, 38, 39], these surface spins have been considered to be deleterious and significant effort has gone into treating and engineering diamond surfaces to minimize their density [40]. However, with proper quantum control, they can be turned into a useful resource. The surface spins can be coherently manipulated and measured, and can be used as the so-called quantum reporters that probe and report the local magnetic environment. For example, by addressing a single surface spin, it is possible to detect and localize proximal single proton nuclear spins on the diamond surface under ambient conditions [28].

The dynamics of individual surface spins are measured by a single near-surface NV center, acting as a nanoscale sensor of magnetic fields created by the surface spins. NV centers are addressed using a confocal microscopy setup, combined with radiofrequency (RF) spin drive fields that are delivered via a transmission line fabricated on a glass coverslip. The surface spin transitions can be addressed with RF pulses delivered in the

same manner. The 2.87 GHz zero-field splitting of the NV center enables independent addressing of the NV spin and the surface spin transitions by using different resonant RF tones at a given bias magnetic field, aligned with the NV axis (z-axis), fig. 1(a), inset. The magnetic dipole coupling between the NV center and the surface spin ensemble is characterized using a double electron-electron resonance (DEER) sequence, fig. 1(b). The NV center spin-echo decays on the timescale $T_2^{(nv)}$, but when a π-pulse flips the surface spins simultaneously with the NV spin, the NV spin echo collapses on a timescale that depends on the strength of the dipolar field created by the surface spins near the NV center. Because the magnetic dipole interaction is long-range, the NV center is, in general, coupled to multiple surface spins, with coupling strengths dependent on locations of surface spins on the diamond surface. The oscillations present in the data at short time (fig. 1(b) red points) indicate that there is one "central" surface spin, whose dipolar coupling strength to the NV center k_{max} dominates over other surface spins. Recent experimental studies have shown that after certain surface treatments, some of the surface spins may be mobile, likely changing their positions under green laser light illumination [41]. We have verified that in our experiments the central surface spin remains in place, even when subjected to green laser light illumination of up to 50 μs [42]. In fact, the central spin position is stable for the experiments carried over the timescale of months. This is likely due to the combination of small photo-ionization cross-section and steric protection by chemical surface groups [41].

Our experiments take place at room temperature, with the bias magnetic field on the order of 1000 G. Therefore the surface spin ensemble is effectively at infinite spin temperature. Nevertheless, we study the dynamics of an individual central surface spin S_j, by measuring its spin autocorrelation functions. Quantum logic gates between the NV center and the central surface spin correlate the NV and the central spin evolution, via their magnetic-dipole interaction, fig. 2(a) [43]. Each measurement consists of a sequence of RF pulses, applied to the NV and surface spins, as well as NV optical spin polarization and readout steps. The RF pulse sequences include two probe segments (CNOT gates), in which the NV center probes the quantum state of the surface spin ensemble, separated by a time interval, in which this state can evolve with control pulses applied to the surface spins (fig. 2(a), grey box). The interpulse spacing t_{NV} of the probe segments is tuned to the timescale of the dipolar interaction between the NV center and the central surface spin so that the final NV center state is contingent on whether the z-projection of the central surface spin changes between the gates. Applying this method, the NV center acts as a probe of central surface spin autocorrelation functions $\langle S_j^{x,y,z}(t) S_j^{x,y,z}(0) \rangle$, where the time t and the measured spin projection depend on the pulses applied during the evolution interval. We performed measurements on 11 separate NV center-surface spin systems [42].

The Ramsey measurement probes fluctuations of the local magnetic field at the central surface spin site (fig. 2(b) blue). The Hahn echo sequence decouples the central surface spin from low-frequency fluctuations, which extends the coherence time to T_2

(fig. 2(b) red). Further decoupling can be achieved with higher-order dynamical decoupling experiments, such as XY-4 (fig. 2(c) blue). However we observe that this does not further increase the coherence time, indicating the presence of a separate decoherence mechanism. The presence of dipolar interactions with other surface spins motivates the MREV-8 experiment, which decouples dipolar interactions. Indeed, we observe that the coherence time in an MREV-8 experiment is extended, compared to the Hahn echo and XY-4 (fig. 2(c) red curve), showing that the dynamics of surface spins are strongly affected by dipolar interactions between them.

In order to understand our observations quantitatively, we consider the effective Hamiltonian in the rotating frame of a single surface spin S_j:

$$H_j = \hbar\gamma_e B_j^z(t) S_j^z + \sum_i \frac{\hbar^2\gamma_e^2}{r_{ij}^3}(1 - 3\cos^2\theta_{ij})[S_i^z S_j^z - \frac{1}{4}(S_i^+ S_j^- + S_i^- S_j^+)], \tag{1}$$

where $\hbar$ is the reduced Planck constant, $\gamma_e = 2\pi \times 2.80$ MHz/G is the electron gyromagnetic ratio, $B_j^z(t)$ is the fluctuating magnetic field at the site of the surface spin, r_{ij} is the distance between the central surface spin j and a different surface spin i, and θ_{ij} is the angle between the direction of the applied external magnetic field and the vector $\boldsymbol{r}_{ij}$. In eq. (1) we do not include the dipolar interaction between the NV center and the central surface spin. By running experiments that vary the NV center spin state during the surface spin evolution period, we find that this interaction does not affect central surface spin evolution within our experimental uncertainty [42].

The strengths of the dipolar interaction terms in eq. (1) vary over different pairs of spins, due to their random positions on the surface. However the $1/r^3$ distance dependence and the 2D nature of the surface spin ensemble imply that it is the proximal surface spins that dominate the spin echo decoherence. We use the spin echo data to extract the strength of the central spin interaction with these proximal spins: $J_1 = 1/T_2 = (0.71 \pm 0.05)\,\mu\text{s}^{-1}$.

Let us consider the origin of the fluctuating local magnetic field B_j^z. All measurements were preformed with the diamond surface submerged in deuterated glycerol. This reduced the density of proton nuclear spins near the surface. However, as observed in several other studies of near-surface NV centers, an intrinsic ~ 1 nm thick layer of surface water and hydrocarbons contains a high density of proton nuclear spins [44, 45, 46]. The periodic features that appear at odd multiples of proton Larmor period in the spin echo, XY-4, and MREV-8 data indicate that these protons are the dominant source of the local field B_j^z. We model the dynamics of B_j^z by parametrizing its power spectrum as a combination of two terms:

$$V(\omega) = \int_{-\infty}^{\infty} \langle B^z(t) B^z(0)\rangle e^{-i\omega t}\, dt = 2\frac{W^2}{\gamma_e^2}\left(\frac{\tau}{\omega^2\tau^2 + 1} + \frac{5}{9}\frac{\tau}{(\omega - \omega_L)^2\tau^2 + 1}\right). \tag{2}$$

The first term, centered at zero frequency, quantifies slow fluctuations with strength W and correlation time τ, due to proton spin projections along the bias magnetic field [42].

The second term quantifies fluctuations near the proton Larmor frequency, due to transverse proton spin projections (fig. 2(d)). We simultaneously fit the Ramsey, spin echo, XY-4, and MREV-8 experimental data shown in fig. 2, with J_1, W, and τ as fit parameters [42]. For this NV-surface spin system, we extract $W = (4.40 \pm 0.38)\ \mu\text{s}^{-1}$ and $\tau = (14.6 \pm 4.2)\ \mu\text{s}$. We note that the decoherence in the Ramsey sequence is significantly faster than that of the spin echo, indicating that W is greater than J_1. The decoherence of the MREV-8 data is dominated by the low-frequency noise component in eq. (2).

Having characterized the local environment of the central surface spin, we study the spin flip-flop transport dynamics in this system by measuring the autocorrelation of the spin component along the applied magnetic field: $\langle S_j^z(t) S_j^z(0)\rangle$, fig. 3(a). The presence of the S^+S^- flip-flop terms in the dipolar interaction in eq. (1) motivates an expectation that this single-spin autocorrelation would decay over the timescale T_z, which is on the order of $1/J_1 = T_2$. In contrast, we consistently observe remarkably slow decay of the longitudinal correlation, which persists over a timescale T_z, in this instance $\sim 30\times$ slower than the dipolar interaction timescale T_2, fig. 2(e). We emphasize that these observations are especially unexpected for individual spin measurements, in contrast with experiments probing a macroscopic spin ensemble (such as a bulk magnetic resonance measurement), where the total spin z-projection is unaffected by flip-flops within the ensemble.

We attribute such anomalously slow relaxation dynamics to the presence of strong disorder. To quantify its effect, we consider a theory model based on an effective single-particle resonance counting. In this model, each spin S_j experiences a time-dependent energy shift owing to the combination of two effective sources of disorder: i) the extrinsic on-site disordered magnetic field $B_j^z(t)$ of typical strength $\sim W$ and ii) the intrinsic local field of strength $\sim J_1$ arising from the Ising component of the dipolar interactions among surface spins. These two components have distinct correlation times and strengths. To quantify the combined dynamical disorder, we introduce the effective disorder strength $W_e = \sqrt{W^2 + J_1^2}$ and the effective disorder correlation time τ_e, defined via $\sqrt{1/\tau_e} = (W\sqrt{1/\tau} + J_1\sqrt{1/T_z})/W_e$ [42]. We assume spins exchange their polarization via dipolar interactions when a pair of spins i, j becomes "resonant", i.e. when the difference between their spin energy shift is smaller than the flip-flop interaction between them, fig. 3(d). Otherwise, energy conservation blocks flip-flops [18]. The spin relaxation dynamics is probed by estimating the probability for a central spin to flip-flop with its neighbor as a function of time. This model predicts that for a 2D dipolar spin system, after averaging over random positioning of spins, the central spin autocorrelation $\langle S_j^z(t) S_j^z(0)\rangle$ decays with an approximate functional form $\exp\left(-(t/T_z)^{2/3}\right)$ [42], where $T_z = \kappa\tau_e W_e/J$. The numerical constant κ is of order unity, and J is the average dipolar interaction strength over the spin ensemble. We compare this prediction with our experimental data by scaling the time axis of the autocorrelation data by independently estimated $\tau_e W_e$, and observe that the data sets for the 7 different NV-central spin systems collapse towards a universal curve, fig. 3(b). Plotting the individual relaxation times T_z versus the product $\tau_e W_e$ reveals the linear relationship predicted by our resonance counting, with the best-fit value

$\kappa = (0.31 \pm 0.14)$ and J = (0.57 ± 0.25) μs^{-1}, consistent with the interaction strengths extracted from the spin echo and XY-4 data sets, fig. 3(c).

To further investigate the role of disorder, we control the magnitude of the effective disorder by spin-lock driving, on resonance with the surface spin Larmor frequency. The resonant drive along the y-axis of the rotating frame adds to the Hamilonian (1) the additional term $H_d = \hbar\Omega S^y$, where Ω is the drive Rabi frequency. We measure the dynamics of the central surface spin projection S_j^y along the driving field, fig. 4(a). This is equivalent to $T_{1\rho}$ measurement in NMR [47, 48]. The relaxation at small Ω is dominated by the local magnetic field noise $B_j^z(t)$, which can flip S_j^y. In this regime, the relaxation rate calculated using the noise model in eq. (2) is consistent with our measurements (fig. 4(b), black line). At large drive strength Ω, spin flips due to $B_j^z(t)$ are suppressed, such that the strength of the effective extrinsic disorder scales as $W^2/(\sqrt{2}\Omega)$. Consequently, the disorder experienced by individual spins is dominated by the Ising component of dipolar interactions along the dressed quantization axis S_j^y. The strength of the latter is reduced to the half of the original Ising interaction along S_j^z in the undriven case [18]. Thus, systematic comparisons of $T_{1\rho}/2$ and T_z enable us to understand the interplay between the extrinsic and intrinsic disorder fields. Shown in fig. 4(c), we find that the relaxation time becomes relatively faster by suppressing the extrinsic disorder when W is sufficiently large. However, for samples with small or intermediate W, the difference in $T_{1\rho}$ and T_z is not substantial, suggesting that the Ising interaction constitutes the dominant source of disorder in this regime. Interestingly, even in this regime, the relaxation rate is approximately a factor of 20 slower than the dipolar interaction scale J_1. This implies that, even in the absence of extrinsic on-site disorder, the intrinsic disorder associated with random positioning of spins is sufficient to strongly suppress spin transport in 2D spin ensemble [42].

A full many-body theoretical treatment of a random dipolar-interacting two-dimensional spin ensemble may be needed to quantitatively predict the relaxation timescale in the absence of extrinsic disorder. A mean-field approach may also provide an approximate solution [49]. It is natural to inquire if a many-body localized phase could be observed for this system. While we do not observe localization directly within the accessible parameter range, we note that theoretical analyses of localization physics typically consider quasi-static disorder models, where the value of on-site field strength does not change on the timescale of a single measurement. Quasi-static disorder generally slows down relaxation as shown in our experiments, but our model demonstrates that time-dependent disorder may speed it up, for a subset of values of W and τ, by allowing previously off-resonant spins to become resonant. Achieving finer control over disorder parameters may allow a detailed single-spin-resolution study of various aspects of localization physics in the present system.

Our observations open the door for in-depth explorations of quantum dynamics in two-dimensional spin systems. In particular, they indicate that systems of interacting spin qubits with long coherence times can be created and manipulated under ambient

conditions at room temperature. Our approach can be used used for the controlled generation of entanglement among spins on the diamond surface with potential applications to quantum sensing and magnetic resonance imaging of single molecules.

References

[1] Kaufman, A. M. *et al.* Quantum thermalization through entanglement in an isolated many-body system. *Science* **353**, 794–800 (2016). URL https://science.sciencemag.org/content/353/6301/794https://science.sciencemag.org/content/353/6301/794.abstract.

[2] Lukin, A. *et al.* Probing entanglement in a many-body-localized system. *Science* **364**, 256–260 (2019). URL https://www-science-org.ezp-prod1.hul.harvard.edu/doi/abs/10.1126/science.aau0818. 1805.09819.

[3] Rispoli, M. *et al.* Quantum critical behaviour at the many-body localization transition. *Nature 2019 573:7774* **573**, 385–389 (2019). URL https://www.nature.com/articles/s41586-019-1527-2.

[4] Morong, W. *et al.* Observation of Stark many-body localization without disorder. *Nature* — **599**, 393 (2021). URL https://doi.org/10.1038/s41586-021-03988-0.

[5] Zhang, J. *et al.* Observation of a Discrete Time Crystal. *Nature* **543**, 217 (2017). 1609.08684.

[6] Choi, J. *et al.* state spin ensemble (a) (b) **vi**, 1–11 (2017).

[7] Keesling, A. *et al.* Quantum Kibble–Zurek mechanism and critical dynamics on a programmable Rydberg simulator. *Nature 2019 568:7751* **568**, 207–211 (2019). URL https://www.nature.com/articles/s41586-019-1070-1.

[8] Ebadi, S. *et al.* Quantum phases of matter on a 256-atom programmable quantum simulator. *Nature 2021 595:7866* **595**, 227–232 (2021). URL https://www.nature.com/articles/s41586-021-03582-4.

[9] Kyprianidis, A. *et al.* Observation of a prethermal discrete time crystal. *Science* **372**, 1192–1196 (2021). URL https://www-science-org.ezp-prod1.hul.harvard.edu/doi/abs/10.1126/science.abg8102. 2102.01695.

[10] Turner, C. J., Michailidis, A. A., Abanin, D. A., Serbyn, M. & Papić, Z. Weak ergodicity breaking from quantum many-body scars URL https://doi.org/10.1038/s41567-018-0137-5.

[11] Bluvstein, D. *et al.* Controlling quantum many-body dynamics in driven Rydberg atom arrays. *Science* **371**, 1355–1359 (2021). URL https://www-science-org.ezp-prod1.hul.harvard.edu/doi/abs/10.1126/science.abg2530.

[12] Kao, W., Li, K. Y., Lin, K. Y., Gopalakrishnan, S. & Lev, B. L. Topological pumping of a 1D dipolar gas into strongly correlated prethermal states. *Science* **371**, 296–300 (2021). URL https://www-science-org.ezp-prod1.hul.harvard.edu/doi/abs/10.1126/science.abb4928.

[13] Cardellino, J. *et al.* The effect of spin transport on spin lifetime in nanoscale systems. *Nature Nanotechnology* **9**, 343–347 (2014).

[14] Alvarez, G. A., Suter, D. & Kaiser, R. Localization-delocalization transition in the dynamics of dipolar-coupled nuclear spins. *Science* **349** (2015).

[15] Wei, K. X., Ramanathan, C. & Cappellaro, P. Exploring Localization in Nuclear Spin Chains. *Physical Review Letters* **120**, 70501 (2018). URL https://link.aps.org/doi/10.1103/PhysRevLett.120.070501.

[16] Smith, J. *et al.* Many-body localization in a quantum simulator with programmable random disorder. *Nature Physics 2016 12:10* **12**, 907–911 (2016). URL https://www.nature.com/articles/nphys3783.

[17] Choi, J.-y. *et al.* Exploring the many-body localization transition in two dimensions. *Science* **352**, 1547–1552 (2016). URL http://www.ncbi.nlm.nih.gov/pubmed/27339981.

[18] Kucsko, G. *et al.* Critical Thermalization of a Disordered Dipolar Spin System in Diamond. *Physical Review Letters* **121**, 23601 (2018). URL https://link.aps.org/doi/10.1103/PhysRevLett.121.023601.

[19] Schreiber, M. *et al.* Observation of many-body localization of interacting fermions in a quasi-random optical lattice (2015). URL http://arxiv.org/abs/1501.05661.1501.05661.

[20] Fel'dman, E. B. & Lacelle, S. Cite as. *J. Chem. Phys* **104**, 2000 (1996). URL https://doi.org/10.1063/1.470956.

[21] Dobrovitski, V. V., Feiguin, A. E., Awschalom, D. D. & Hanson, R. Decoherence dynamics of a single spin versus spin ensemble. *Physical Review B - Condensed Matter and Materials Physics* **77**, 245212 (2008). URL https://journals-aps-org.ezp-prod1.hul.harvard.edu/prb/abstract/10.1103/PhysRevB.77.245212.

[22] Anderson, P. W. Absence of Diffusion in Certain Random Lattices. *Physical Review* **109**, 1492–1505 (1958).

[23] Burin, A. L. Energy delocalization in strongly disordered systems induced by the long-range many-body interaction (2006). URL http://arxiv.org/abs/cond-mat/0611387. 0611387.

[24] Yao, N. Y. *et al.* Many-body localization in dipolar systems. *Physical Review Letters* **113**, 243002 (2014). URL https://journals.aps.org/prl/abstract/10.1103/PhysRevLett.113.243002.

[25] Gong, Z.-X., Foss-Feig, M., Brandão, F. G. S. L. & Gorshkov, A. V. Entanglement Area Laws for Long-Range Interacting Systems. *Physical Review Letters* **119**, 50501 (2017). URL http://link.aps.org/doi/10.1103/PhysRevLett.119.050501.

[26] Orioli, A. P. *et al.* Relaxation of an Isolated Dipolar-Interacting Rydberg Quantum Spin System. *Physical Review Letters* **120**, 063601 (2018). 1703.05957.

[27] Gopalakrishnan, S., Agarwal, K., Demler, E. A., Huse, D. A. & Knap, M. Griffiths effects and slow dynamics in nearly many-body localized systems. *Physical Review B* **93**, 1–12 (2016). 1511.06389.

[28] Sushkov, A. O. *et al.* Magnetic resonance detection of individual proton spins using quantum reporters. *Physical Review Letters* **113**, 197601 (2014). URL https://journals-aps-org.ezp-prod1.hul.harvard.edu/prl/abstract/10.1103/PhysRevLett.113.197601.

[29] Davis, E. J. *et al.* Probing many-body noise in a strongly interacting two-dimensional dipolar spin system (2021). URL http://arxiv.org/abs/2103.12742. 2103.12742.

[30] Grotz, B. *et al.* Sensing external spins with nitrogen-vacancy diamond. *New Journal of Physics* **13**, 55004 (2011).

[31] Grinolds, M. S. *et al.* Subnanometre resolution in three-dimensional magnetic resonance imaging of individual dark spins. *Nature Nanotechnology* **9**, 279–284 (2014). URL www.nature.com/naturenanotechnology. 1401.2674.

[32] Tetienne, J. P. *et al.* Spin properties of dense near-surface ensembles of nitrogen-vacancy centers in diamond. *Physical Review B* **97**, 085402 (2018). URL https://journals-aps-org.ezp-prod1.hul.harvard.edu/prb/abstract/10.1103/PhysRevB.97.085402. 1711.04429.

[33] Sangtawesin, S. *et al.* Origins of Diamond Surface Noise Probed by Correlating Single-Spin Measurements with Surface Spectroscopy **031052**, 1–17 (2019).

[34] Stacey, A. *et al.* Evidence for Primal sp ¡sup¿2¡/sup¿ Defects at the Diamond Surface: Candidates for Electron Trapping and Noise Sources. *Advanced Materials Interfaces* **6**, 1801449 (2019). URL http://doi.wiley.com/10.1002/admi.201801449.

[35] Rosskopf, T. *et al.* Investigation of Surface Magnetic Noise by Shallow Spins in Diamond **147602**, 1–5 (2014).

[36] Romach, Y. *et al.* Spectroscopy of Surface-Induced Noise Using Shallow Spins in Diamond. *Physical Review Letters* **114**, 17601 (2015). URL `https://link.aps.org/doi/10.1103/PhysRevLett.114.017601`.

[37] Myers, B. A. *et al.* Probing Surface Noise with Depth-Calibrated Spins in Diamond. *Physical Review Letters* **113**, 27602 (2014).

[38] Myers, B. A., Ariyaratne, A. & Jayich, A. B. Double-Quantum Spin-Relaxation Limits to Coherence of Near-Surface Nitrogen-Vacancy Centers. *Physical Review Letters* **118**, 197201 (2017).

[39] Bluvstein, D., Zhang, Z., McLellan, C. A., Williams, N. R. & Jayich, A. C. Extending the Quantum Coherence of a Near-Surface Qubit by Coherently Driving the Paramagnetic Surface Environment. *Physical Review Letters* **123**, 146804 (2019). URL `https://journals-aps-org.ezp-prod1.hul.harvard.edu/prl/abstract/10.1103/PhysRevLett.123.146804`. `1905.06405`.

[40] Fávaro de Oliveira, F. *et al.* Tailoring spin defects in diamond by lattice charging. *Nature Communications* **8**, 15409 (2017). URL `http://www.nature.com/doifinder/10.1038/ncomms15409`.

[41] Dwyer, B. L. *et al.* Probing spin dynamics on diamond surfaces using a single quantum sensor (2021). URL `http://arxiv.org/abs/2103.12757`. `2103.12757`.

[42] *Supplementary Information*.

[43] Laraoui, A. *et al.* High-resolution correlation spectroscopy of 13C spins near a nitrogen-vacancy centre in diamond. *Nature Communications* **4**, 1–7 (2013). URL `www.nature.com/naturecommunications`.

[44] Staudacher, T. *et al.* Probing molecular dynamics at the nanoscale via an individual paramagnetic centre. *Nature Communications* **6**, 8527 (2015).

[45] Loretz, M. *et al.* Single-proton spin detection by diamond magnetometry. *Science* science.1259464—- (2014).

[46] DeVience, S. J. *et al.* Nanoscale NMR spectroscopy and imaging of multiple nuclear species. *Nature Nanotechnology* **10**, 129–134 (2015). URL `http://www.nature.com/articles/nnano.2014.313`.

[47] Abragam, A. The Principles of Nuclear Magnetism: The International Series of Monographs on Physics (1961).

[48] Slichter, C. P. *Principles of Magnetic Resonance*, vol. 1 of *Springer Series in Solid-State Sciences* (Springer Berlin Heidelberg, Berlin, Heidelberg, 1978). URL `http://link.springer.com/10.1007/978-3-662-12784-1`.

[49] Gräßer, T., Bleicker, P., Hering, D.-B., Yarmohammadi, M. & Uhrig, G. S. Dynamic mean-field theory for dense spin systems at infinite temperature (2021). URL `https://arxiv.org/abs/2107.07821v1`. `2107.07821`.

Acknowledgements:

The authors acknowledge discussions with Timo Gräßer, Götz Uhrig, Elana Urbach, Tamara Sumarac, Emma Rosenfeld, Bo Dwyer, Harry Zhou, and Oleg P. Sushkov. This work was supported by the National Science Foundation grant PHY-2014094, NSF, CUA, ARO MURI, and Moore Foundation.

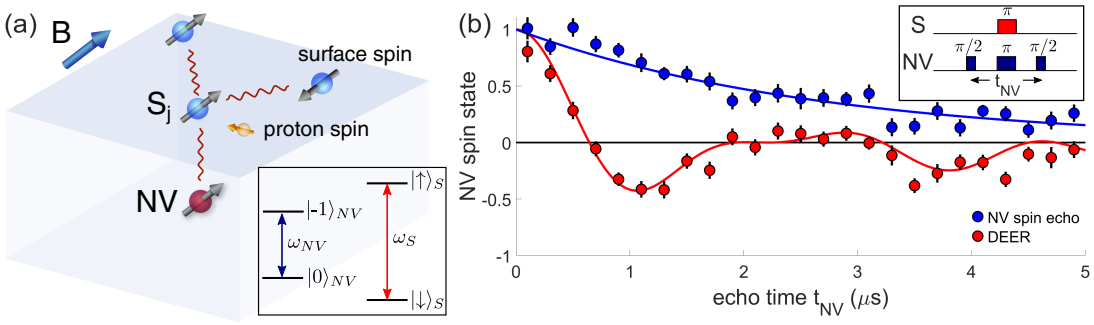

Figure 1: Characterization of a representative NV center - surface spin system. (a) The experimental platform consists of a single, shallow NV center strongly coupled to one surface electron spin S_j. Other electron spins and proton nuclear spins reside on the surface of the diamond. An external magnet splits the electron and nuclear spin states and allows independent manipulation of NV center and surface spins at their corresponding magnetic resonance frequencies. Inset: NV center and surface spin level structure. NV center transition is addressed at angular frequency ω_{NV} while surface spin transition is addressed at ω_S. (b) NV center Hahn echo (blue) and double electron-electron resonance (DEER) (red) measurements. The oscillations present in the DEER data indicate that the magnetic dipole interactions of this NV center with the surface spin ensemble are dominated by a central surface spin with the coupling strength $k_{max} = (4.90 \pm 0.57)\ \mu\text{s}^{-1}$ (red line fit). Inset: the DEER pulse sequence.

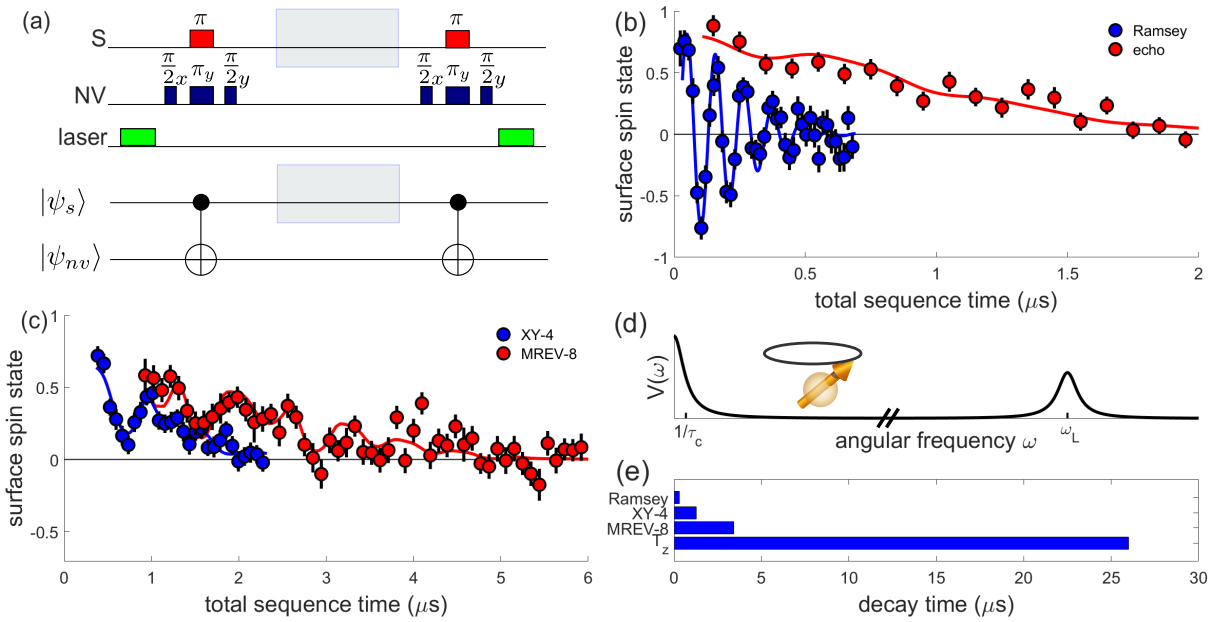

Figure 2: Characterization of the local magnetic environment of a central surface spin. (a) Top: the correlation spectroscopy pulse sequence. In our experiments the NV center interpulse spacing is set such that the NV center is primarily sensitive to the central surface spin autocorrelation. Manipulating the surface spins during the gray shaded region allows us to measure different central surface spin correlation functions. The complete pulse sequences for all measurements are described in SI. Bottom: Quantum logic gate representation of the correlation spectroscopy pulse sequence. The two CNOT gates are applied, such that the final state of the NV center is contingent on whether the z-projection of the central surface spin changed during the time between the gates. (b) Surface spin detuned Ramsey (blue) and Hahn echo (red) measurements of $\langle S_j^x(t)S_j^x(0)\rangle$ transverse central spin autocorrelation. The Hahn echo decay time is $T_2 = (1.41 \pm 0.11)$ μs and the Ramsey decay time is $T_2^* = (0.32 \pm 0.02)$ μs. Solid lines are fits using the model in eqs. (1,2). The oscillations in the Ramsey data are due to the 9.2 MHz detuning from the surface spin Larmor frequency. (c) Surface spin XY-4 measurement (blue) and MREV-8 measurement (red). The MREV-8 measurement is performed within a spin echo (see SI for full pulse sequences). Solid lines are fits using our model. The oscillations present in both measurements are due to proton nuclear spin precession. (d) Nuclear spin bath noise power spectrum V(ω), with peaks at zero frequency and proton Larmor frequency ω_L. (e) The full characterization of relaxation timescales for one of the central surface spin systems, including the Ramsey, XY-4, MREV-8, and S^z autocorrelation measurements.

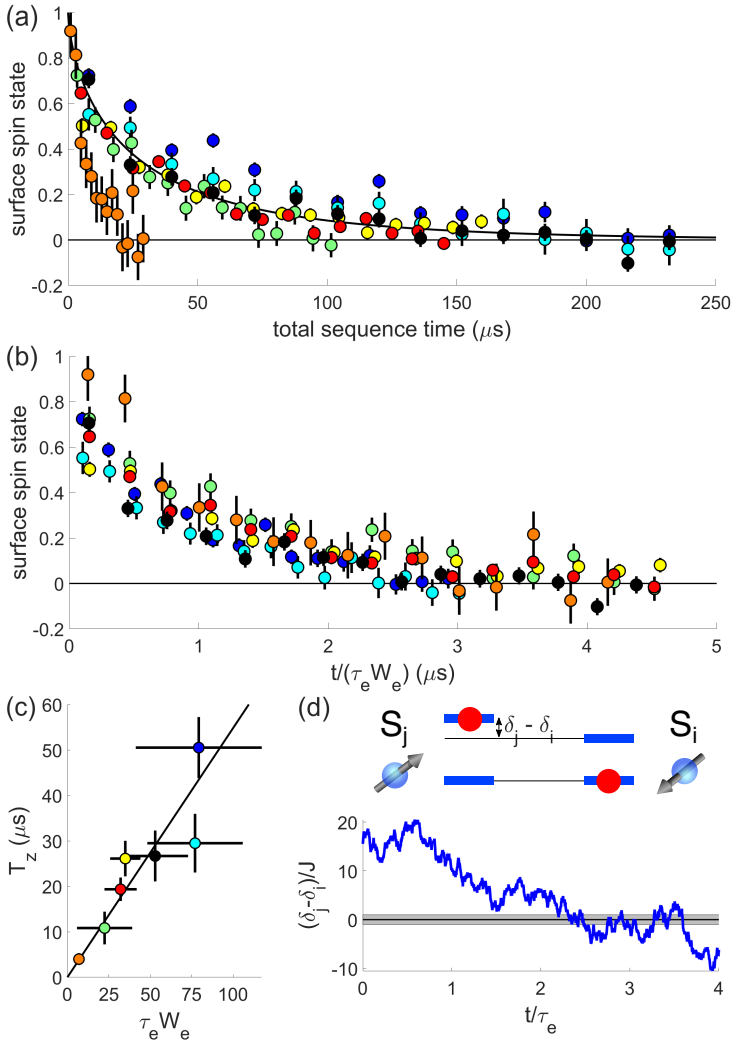

Figure 3: Measurements of central surface spin $\langle S_j^z(t)S_j^z(0)\rangle$ autocorrelation. (a) S^z autocorrelation measurements for 7 different central surface spin systems. The black line is a stretched-exponential fit to one of the data sets, from which we extract the relaxation time T_z. (b) S_z autocorrelation measurements with the delay time re-scaled by the product $\tau_e W_e$ of the effective disorder correlation time and disorder width, independently measured for each surface spin system. We observe a collapse of the 7 data sets to a universal stretched-exponential decay curve, in agreement with our dynamical disorder model. (c) S_z autocorrelation decay time plotted as a function of the product $\tau_e W_e$, with the linear fit shown by the black line. (d) A schematic of the spin hopping process in our model, showing a central surface spin S_j and another surface spin S_i. Each spin state is shifted by time-dependent on-site detuning δ (blue line), due to the local dynamical disorder created by nuclear spin bath noise and Ising dipolar interaction terms. The spins can flip-flop if their detunings differ by less than the strength J of the dipolar interaction between them (grey band).

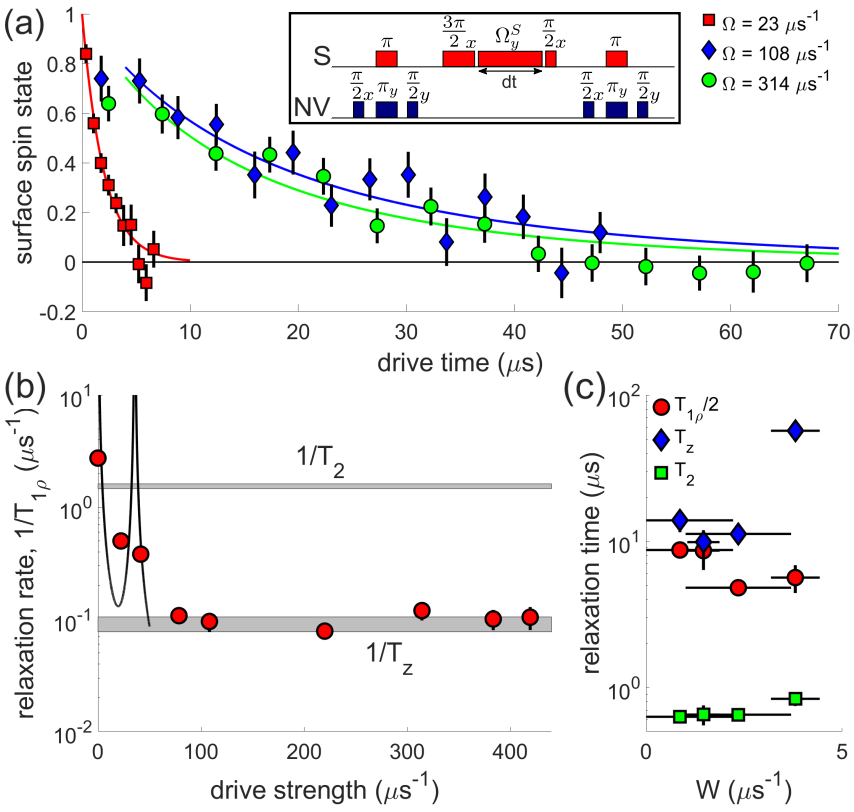

Figure 4: Evolution of central surface spin under spin-lock driving. (a) Measurements of $\langle S_j^y(t)S_j^y(0)\rangle$ autocorrelation under spin-lock driving for different drive strengths. Stronger driving results in better decoupling from the nuclear spin bath magnetic noise and longer $T_{1\rho}$ relaxation time. For drive strength $\Omega \gtrsim 50\,\mu\text{s}^{-1}$, relaxation rate is independent of Ω. Lines show stretched exponential decay fits. Inset: radio frequency NV and surface spin pulses; green laser polarization and readout pulses applied before and after this sequence of RF pulses. (b) Spin-lock driving relaxation rate as a function of drive strength for the surface spin system presented in (a), along with the corresponding decay rates for Hahn echo ($1/T_2$) and S^z autocorrelation ($1/T_z$) experiments, shown by the gray bands. The point at $\Omega = 0$ corresponds to the decay of the Ramsey coherence ($1/T_2$*). The measurements performed with drive strength below 50 μs^{-1} are consistent with direct relaxation due to the nuclear spin bath noise with spectrum $\text{V}(\omega)$. Relaxation rates for drive strengths $\Omega \gtrsim 50\,\mu\text{s}^{-1}$ are independent of Ω and consistently much slower than the dipolar interaction scale $1/T_2$. (c) Comparison between different autocorrelation decay timescales for 4 different surface spin systems. Red circles, labeled $T_{1\rho}/2$, show the decay time under spin-lock at strong driving. As the dynamical on-site disorder strength W increases, the T_z autocorrelation decay time increases compared with the autocorrelation decay at strong driving with suppressed disorder ($T_{1\rho}/2$). Both of these decays are much slower (by a factor of ≈ 30) than the dipolar interaction scale, given by T_2.